HADMAR'2001, 22nd Int. Conference on Hydrodynamics and Aerodynamics in Marine Engineering,
1-4 October 2001, Varna, Bulgaria.

Report 1287-P, October 2001,
Delft University of Technology,
Ship Hydromechanics Laboratory,
Mekelweg 2, 2628 CD Delft,
The Netherlands.

Reprinted: 05-10-2001.
Website: www.shipmotions.nl

HYDRODYNAMIC TRANSVERSE LOADS ON SHIPS IN DEEP AND SHALLOW WATER

W. Beukelman and J.M.J. Journée
Delft University of Technology

1. Abstract

In general the character of the transverse forces may be distinguished in a potential and a viscous part.
A calculation method will be presented to determine the potential forces. These forces may be determined by the rate of change of fluid momentum, which is a very significant characteristic for calculating motions of ships in waves, slamming, lift forces on hull and rudder and manoeuvring derivatives. The drift angular dependence for the potential transverse forces appears to be proportional to $0.5 \cdot \sin 2\beta$. At small drift angles up to $\beta = 10^0$, this dependence may be considered to be linear with β and may be applied for manoeuvring. These force coefficients will be compared with experimental results for a ship-like wing model in deep and shallow water as well as with those of a segmented ship model in the same conditions.
In this case of small drift angles the linear potential part of the transverse force is dominant, especially in shallow water. Then the viscous part may be neglected. The maximum value of the potential transverse force will appear at drift angle $\beta = 45^0$; see Figure 1.

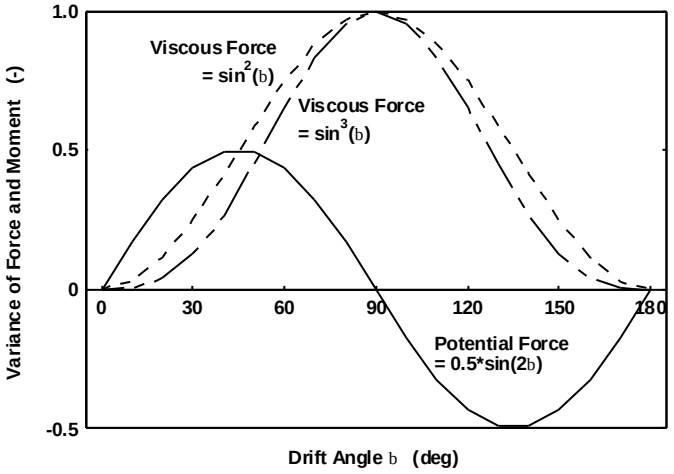

Figure 1 Angular dependence of potential and viscous forces

The viscous transverse force has a drift angular dependence according to $\sin^2 b$ (Version 1) or to $\sin^3 b$ (Version 2), which for small drift angles may considered being approximated by b^2 or b^3, showing in this way a non-linear character in this region. The maximum value of this viscous force will be achieved at drift angle $b = 90^0$, where the potential force will be zero. In this respect reference is made to tests with a segmented ship model at transverse speed in deep water. Determination of the amplitude of the viscous force from tests at small drift angles appeared to be questionable.
Regions of drift angles will be indicated where both potential and viscous forces should be taken into account.

2. Calculation procedures

2.1. General

The potential forces and moments are calculated by the exchange of fluid momentum according to the method as proposed by Jones [1], Payne [2] and Newman [3].
The determination of added mass and damping is derived for an ideal fluid. This means that this fluid is incompressible, irrotational and inviscid. For such a fluid the Bernoulli equation relates the pressure with the velocities. The flow around the ship is represented by a distribution of sources and sinks only. The equations of motion in the flow are the equivalent of Newton's second law.
The sectional added mass m' is determined by using a method based upon the potential theory only, as presented by Keil [4] including the influence of restricted water depth. This method has been incorporated in the ship motions computer program SEAWAY of Journée as described in [5]. With aid of this computer program the hydromechanical derivatives are determined according to expressions derived in the following sections.
The sectional added mass m' may also be obtained by a diffraction method, i.e. DELFRAC of Pinkster as presented by Dmitrieva in [6]. The advantage of this method is that wall influence or influence of other obstacles in the neighbourhood may be taken into account too.
To compute the flow around an arbitrary profile, De Koning Gans [7] developed a higher order three-dimensional panel method program. His method has also been applied to determine the pressure distribution around a wing profile and may also be used to calculate the normal and lift forces.

2.2. Potential transverse forces

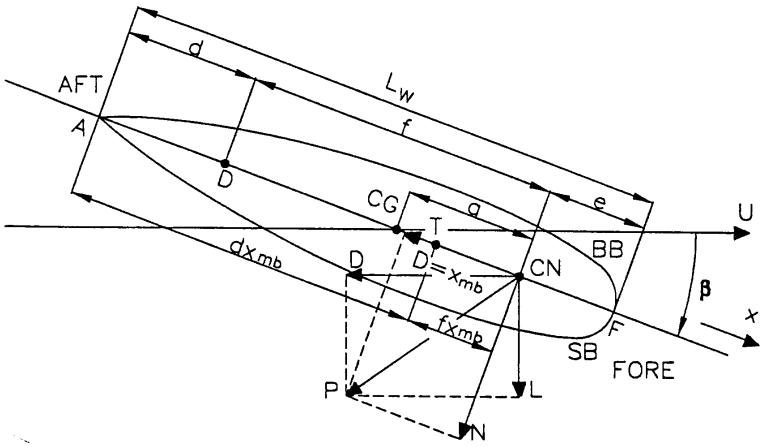

Figure 2 Forces acting on a wing section

The calculation of the transverse force, based on the rate of change of fluid momentum, is applied to determine the lift forces on a wing profile. For zero drift angles the transverse force N is equal to the lift force L; see Figure 2.

The hydromechanical manoeuvring coefficients are derived from the transverse forces and moments. In this way a ship should considered to be a wing profile with a low aspect ratio.

The derivative of the local potential normal or transverse force N_{pot} in longitudinal direction may be set equal to the time derivative of the local added mass impulse in transverse direction - also known as the fluid momentum exchange - and is presented as:

$$\frac{dN_{pot}}{dx} = \frac{d}{dt}(m'v)$$

Equation 1

with: m' added mass in transverse direction per unit length
$v = U \sin b$ transverse component of the flow speed $-U$ (opposite to the towing direction)
b drift angle or angle of attack.

Equation 1 may be developed into:

$$\frac{dN_{pot}}{dx} = \frac{dm'}{dx}\frac{dx}{dt}v + m'\frac{dv}{dx}\frac{dx}{dt}$$

Equation 2

Keeping in mind that $dv/dx = 0$ and $dx/dt = -U\cos b$ ($-U$ being the fluid flow speed on the wing which is opposite to the wing model speed), the expression becomes:

$$\frac{dN_{pot}}{dx} = -U^2 \sin b \cos b \frac{dm'}{dx}$$

Equation 3

or:

$$dN_{pot} = -\frac{1}{2}U^2 dm' \sin 2b$$

Equation 4

The total normal force on the wing model will be obtained by integration of dN_{pot} over the length (chord) of the wing as:

$$N_{pot} = \int_A^F dN_{pot} = -\frac{1}{2}U^2 \sin 2b \int_A^F dm' = -\frac{1}{2}U^2 \sin 2b\,[m'_F - m'_A]$$

Equation 5

If $m'_F = m'_A = 0$, which is generally the case, the total transverse force will be zero. This phenomenon is quite in accordance with d'Alembert's paradox on the assumption that the flow is irrotational in an ideal fluid without viscosity, vortex streets and separation. Only for a body with a tail fin at the end, so $m'_A \neq 0$, the situation is fundamentally different as stated by Newman in [3]. A trailing vortex street may originate from the abrupt trailing edge at the tail. It remains, however, questionable why this 'tail effect' may not be expected earlier along the body in a real fluid. It is well known that viscosity is required to start the potential lift production. Jones [1] put forward that with the aid of the Kutta condition it might be easily shown that sections of the wing behind the section with the largest width develop no lift. Katz and Plotkin [8] even showed that there would be no lift if the beam $b(x)$ were constant with x. Integration up to the section with the maximum width should be sufficient.
If the integration in Equation 5 is carried out from the forward point (F) to the section with the maximum beam at x_{mb} and $m'_F = 0$, then it holds that the transverse force may be written as:

$$N_{pot} = \frac{1}{2}U^2 m'_{x_{mb}} \sin 2b$$

Equation 6

Equation 6 shows that the potential transverse force with respect to the drift angle b oscillates according to $\sin 2b$; see also Figure 1.

2.2.1. Potential transverse moments

The moment of the local transverse force with respect to the origin of a body-fixed right hand co-ordinate system x, y, z (x longitudinal, positive in forward speed direction at $b = 0^0$, y transverse, positive to the right or starboard side SB, z positive downwards) may be expressed as follows:

$$dM_{pot} = \frac{dN_{pot}}{dx} x dx$$

Equation 7

With the origin of the co-ordinate situated at arbitrary location D (Figure 2) and substituting Equation 4 into Equation 7 the total moment of the transverse force on the wing model with respect to D will be:

$$M_{pot} = \int_D^F dM_{pot} = -\frac{1}{2}U^2 \sin 2b \int_D^F x dm'$$
$$= -\frac{1}{2}U^2 \sin 2b \left\{ xm' \Big|_D^F - \int_D^F m' dx \right\}$$

Equation 8

It follows with $m'_F = 0$:

$$M_{pot} = \frac{1}{2} U^2 m_D \sin 2b$$

Equation 9

Following the reasoning as used for the transverse or lift force, point D should be chosen as located at x_{mb} (Figure 2) and so:

$$m_D = m_{x_{mb}} = \int_{D=x_{mb}}^{F} m' dx$$

Equation 10

is the added mass from F to x_{mb}.

Analogous to the situation of the transverse potential force (Equation 6), it also holds for the transverse potential moment (Equation 9) that this moment also vary with respect to the drift angle b according to $\sin 2b$.

The moment M_{pot} (Equation 9) with respect to CG delivers the well known destabilising Munk moment for a body with a drift angle at a steady translation. Except for the integration boundaries, this expression agrees with that one found by Faltinsen [9].

The distance $f_{x_{mb}}$ from D ($x = x_{mb}$) to CN is found as follows:

$$f_{x_{mb}} = \frac{M_{pot}}{N_{pot}} = \frac{m_{x_{mb}}}{m'_{x_{mb}}}$$

Equation 11

The distance e from CN to the forward wing point F will be:

$$e = L_w - d_{x_{mb}} - f_{x_{mb}} = L_w - d_{x_{mb}} - \frac{m_{x_{mb}}}{m'_{x_{mb}}}$$

Equation 12

from which follows:

$$\frac{e}{L_w} = \frac{L_w - d_{x_{mb}} - \dfrac{m_{x_{mb}}}{m'_{x_{mb}}}}{L_w}$$

Equation 13

2.2.2. Potential transverse forces and moments at small drift angles

For small drift angles to about 10 degrees it may be assumed that $\frac{1}{2}\sin 2b \approx b$ and the transverse force (Equation 6) becomes:

$$N_{pot} = U^2 b \; m'_{x_{mb}}$$

Equation 14

while the transverse moment according to Equation 9 and Equation 10 results into:

$$M_{pot} = U^2 b \; m_{x_{mb}}$$

Equation 15

In the range of drift angles from 0 to 10 degrees, it is obvious from Equation 14 and Equation 15, that the potential drift force and moment may be characterised as linear with the drift angle b. If the moment M_{pot} of Equation 9 is presented as the Munk moment, the transverse force N_{pot} of Equation 6 should be the equivalent of the Munk force.

2.2.3. Potential lift forces and moments

At very small drift angles to about $b = 4^0$, the lift force L may be put equal to the transverse force N_{pot}; see Figure 2. For larger drift angles the longitudinal force T should accounted for to find the lift force L and drag D, as denoted in Section 3.2.
The lift force coefficient is presented as:

$$C_L = \frac{L}{\frac{1}{2} r U^2 L_w T_w}$$

Equation 16

in which L_w is the length of the wing or ship and T_w is the draught.
Using Equation 14, the slope of the lift curve at $b = 0^0$ (so $L = N_{pot}$) may be presented as:

$$\frac{\partial C_L}{\partial b} = \frac{m'_{x_{mb}}}{\frac{1}{2} r L_w T_w}$$

Equation 17

The moment of the lift force at $b = 0^0$ with respect to the forward wing point F is, using Equation 14 and Equation 15:

$$M^e_{pot} = N_{pot} \cdot e = U^2 b m'_{x_{mb}} \left(L_w - d_{x_{mb}} - \frac{m_{x_{mb}}}{m'_{x_{mb}}} \right)$$

Equation 18

The moment coefficient is presented as:

$$C^e_{M_{pot}} = \frac{M^e_{pot}}{\frac{1}{2} r U^2 L_w{}^2 T_w}$$

Equation 19

Substitution of Equation 18 into Equation 19 delivers the slope of the moment curve at $b = 0^0$:

$$\frac{\partial C^e_{M_{pot}}}{\partial b} = \frac{m'_{x_{mb}}}{\frac{1}{2} r L_w T_w} \cdot \frac{e}{L_w} = \frac{\partial C_L}{\partial b} \cdot \frac{e}{L_w}$$

Equation 20

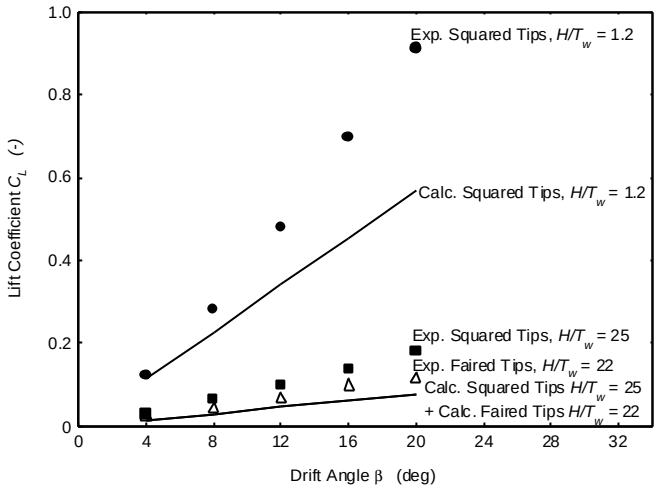

Figure 3 Lift coefficients for wing model T_w=0.10 m, Fn=0.20

Tests with a wing model as reported in [10] show that lift and drag increase strongly as the water depth reduces; see Figure 3 as an example of the lift coefficients. Using faired tips at the bilge instead of square tips decreases lift and drag considerably. Results of experiments with faired tips approach the calculated potential linear values, for both lift and moment in case of very small angles of attack.

2.2.4. Manoeuvring

2.2.4.1. General

For manoeuvring it is assumed that the horizontal ship motions are small around the direction of the forward ship speed U, so that the forces may be considered to be linear with respect to the drift angle b. For that case only potential forces are taken into consideration.

The manoeuvring coefficients will be calculated with aid of seakeeping coefficients; see for a description [11,12,13]. These coefficients generally are built up from terms with sectional fluid added mass (m') and damping coefficient ($N'–U\,dm'/dx$). For manoeuvring it is assumed that the oscillation is almost zero, so that the damping coefficient $N' \rightarrow 0$. The term $U\,dm'/dx$ of the damping coefficient will deliver the transverse forces as shown before. For this reason terms with $U\,dm'/dx$ will be integrated from the forward point F to the section with the maximum beam at x_{mb}. This holds also for terms with pure added mass m' following from $U\,dm'/dx$ by partial integration. Terms with pure added mass m', so in case of acceleration, will be integrated over the whole model or ship length L_w.

The historic relation between seakeeping and manoeuvring has to be considered to find expressions for the manoeuvring coefficients. The most remarkable difference is the choice of the vertical axis z, positive upwards in seakeeping and downwards for manoeuvring. Because of similar longitudinal axes in the ship's forward direction, the transverse axis is also different in direction, positive to PS for seakeeping and to SB for manoeuvring.

2.2.4.2. Sway

The equation of motion for sway related to seakeeping may be written as:

$$(m_w + a_{yy})\ddot{y} + b_{yy}\dot{y} = Y_a \sin(wt + e)$$

Equation 21

where m_w is the mass of wing or ship and a_{yy} and b_{yy} are the seakeeping coefficients for added mass and damping, respectively.
Substituting $y = y_a \sin wt$ delivers for the quadrature component of the side force:

$$b_{yy} w y_a = Y_a \sin e$$

Equation 22

The sway oscillation for manoeuvring may be presented as:

$$(Y_{\dot{v}} - m_w)\dot{v} + Y_v v = Y_a \sin(wt + e)$$

Equation 23

from which follows:

$$Y_v w y_a = -Y_a \sin e$$

Equation 24

The sign for this force is opposite to that found for seakeeping due to the difference in the direction of the y axis. In the above equation are $Y_{\dot{v}}$ and Y_v the manoeuvring coefficients for added mass and damping, respectively.
With aid of the expressions for the seakeeping coefficients as presented in [11,12,13], it follows with Equation 21, Equation 22 and Equation 24 that:

$$Y_v = -b_{yy} = U \int_{x_{mb}}^{F} \frac{dm'}{dx} dx = -U m'_{x_{mb}}$$

Equation 25

In non-dimensional form this expression becomes:

$$Y'_v = \frac{Y_v}{\frac{1}{2} r L_w^2 U} = \frac{m'_{x_{mb}}}{\frac{1}{2} r L_w^2}$$

Equation 26

In the same way, it is found:

$$Y_{\dot{v}} = -a_{yy} = -\int_{A}^{F} m' dx$$

Equation 27

which becomes in non-dimensional form:

$$Y'_{\dot{v}} = \frac{Y_{\dot{v}}}{\frac{1}{2} r L_w^3} = -\frac{1}{\frac{1}{2} r L_w^3} \int_{A}^{F} m' dx$$

Equation 28

The other coefficients for sway may be determined in a similar way. An overview of these coefficients is presented in Table 7 in the Appendix. An example of the measured and calculated coefficient Y'_v is presented in Figure 4 and Figure 5 in Section 3.2.

2.2.4.3. Yaw

The yawing motion in manoeuvring may be divided in sway and yaw with a mutual phase difference of 90 degrees. This motion may be obtained by forced oscillation in such a way that the velocity vector of CG is tangent to the swaying path of CG, which is achieved by adjusting a phase angle Φ between the fore and aft leg in case of an oscillator, see [11,12,13], so that:

$$tg\frac{\Phi}{2} = \frac{lw}{2U}$$

Equation 29

where l is the distance between the oscillator legs.
The force equation for sway and yaw may be written as:

$$(m_w + a_{yy})\ddot{y} + b_{yy}\dot{y} + d_{yy}\ddot{y} + e_{yy}\dot{y} = Y_a \cos(wt + e)$$

Equation 30

The force here is taken in phase with the yawing angle y and negative in sign in view of the manoeuvring notation.
Substitution of $y = y_a \sin wt$ and:

$$y = y_a \cos wt = \frac{2y_a}{l}\sin\frac{\Phi}{2}\cos wt$$

Equation 31

in Equation 30 and using the pure yawing motion equation:

$$Y_r\dot{r} + (Y_r - m_w U)r = Y_a \cos(wt + e)$$

Equation 32

yields:

$$(Y_r - m_w U) = \frac{Y_a \sin e}{y_a w} = \frac{-w^2(m_w + a_{yy})y_a - e_{yy} w y_a}{y_a w}$$

or:

$$Y_r = -e_{yy} - \frac{w(m_w + a_{yy})l}{2\sin\frac{\Phi}{2}} + m_w U$$

Equation 33

If $w \to 0$ then: $\sin\frac{\Phi}{2} \to tg\frac{\Phi}{2} \to \frac{\Phi}{2} \to \frac{lw}{2U}$, which results into:

$$Y_r = -e_{yy} - Ua_{yy}$$

Equation 34

Using the seakeeping expressions for e_{yy} and a_{yy} as presented in [11] and taking the damping $N' \to 0$ for $w \to 0$ delivers:

$$Y_r = U\left[\int_{x_{mb}}^{F}\frac{dm'}{dx}xdx + \int_{A}^{F}m'dx\right]$$

Equation 35

In non-dimensional form after partial integration is found:

$$Y'_r = \frac{Y_r}{\frac{1}{2} r L_w^3 U} = \frac{1}{\frac{1}{2} r L_w^3} \left[- x_{mb} m'_{x_{mb}} - \int_{x_{mb}}^{F} m' dx + \int_{A}^{F} m' dx \right]$$

Equation 36

The in-phase relation of Equation 30 and Equation 32 gives in a similar way:

$$Y_{\dot{r}} = -d_{yy} + \frac{b_{yy} U}{w^2}$$

Equation 37

and, after taking the damping $N' \rightarrow 0$ for $w \rightarrow 0$, it remains:

$$Y_{\dot{r}} = \int_{A}^{F} m' x dx = N_{\dot{v}}$$

Equation 38

Non-dimensional presentation provides:

$$Y'_{\dot{r}} = N'_{\dot{v}} = - \frac{1}{\frac{1}{2} r L_w^4} \int_{A}^{F} m' x dx$$

Equation 39

The other coefficients may be determined in a similar way. In these equations, d_{yy} and e_{yy} are the seakeeping moment coefficients for respectively added mass and damping.
An overview of the yaw coefficients is presented in Table 8 in the Appendix.

2.2.4.4. Semi-empirical methods

Manoeuvring coefficients	*Fn*	Experiment		Present Calculation	Semi-empirical methods			
		Square Tips	Faired Tips		Clarke	Inoue	Norrbin	Gerritsma Beukelman Glansdorp
$-Y'_{\dot{v}} *10^2$	.15 .20 .25	0.92 1.04 1.25	0.85 0.82 0.64	0.89	0.77	0.90	0.90	0.90
$-Y'_v *10^2$	.15 .20 .25	2.15 2.18 2.02	1.39 1.18 1.50	0.97	1.17	0.96	1.08	0.96
$-N'_{\dot{v}} *10^2$	.15 .20 .25	-0.11 -0.13 -0.11	-0.09 -0.05 -0.17	-0.05	0.02	-0.05	-0.05	-0.05
$-N'_v *10^2$	.15 .20 .25	0.46 0.46 0.57	0.26 0.22 0.28	0.40	0.37	0.39	0.38	0.68

$-Y'_{\dot{r}}$ $*10^2$	.15 .20 .25	-0.05 0.16 0.12	0.05 0.12 0.21	-0.05	0.04	-0.05	-0.05	-0.05
$-Y'_{r}$ $*10^2$	.15 .20 .25	-0.47 -0.38 -0.66	-0.31 -0.21 -0.33	-0.50	-0.27	-0.37	-0.24	-0.24
$-N'_{\dot{r}}$ $*10^2$	.15 .20 .25	0.01 -0.03 -0.07	0.10 0.10 0.16	0.07	0.04	0.07	0.07	0.07
$-N'_{r}$ $*10^2$	.15 .20 .25	0.24 0.27 0.27	0.14 0.16 0.13	0.22	0.18	0.21	0.21	0.15

Table 1 Comparison of measured, calculated and semi-empirical values for the manoeuvring coefficients (T_w = 0.10 m, H = 2.50 m)

The Delft University of Technology started its experimental investigations on manoeuvring in the late sixties; see van Leeuwen and Journée [14]. Several attempts have been published in the past in literature to find empirical expressions for the manoeuvring coefficients of ships based on measured values from planar motion and rotating arm experiments. Mentioned here are Norrbin (1971) [15], Gerritsma et.al. (1974) [16] and Inoue et.al. (1981) [17].
Clarke et.al. (1982) [18] compared several empirical formulas against scatter plots of velocity derivatives. Clarke used multiple linear regression analysis to develop empirical formulas to explain the variation in the available data for the velocity derivatives and also the acceleration derivatives. His resulting four equations for velocity derivatives were obtained from the pooled data and are together with the remaining equations for acceleration derivatives also presented in [19].
Table 1 shows the experimental results of the manoeuvring derivatives for the ship-like condition T_w = 0.10 m, H = 2.50 m (deep water) compared to the present calculation results and the semi-empirical methods mentioned above.

2.3. Viscous transverse forces and moments

For $b = 0^0$ the drag force in the longitudinal direction is mainly due to frictional forces, while the wave forces are neglected for low forward speed. There are well known expressions to determine this longitudinal resistance force on a ship. For larger drift angles the transverse viscous current force and moment on the ship can be determined using the cross flow principle as long as the current direction is not close to the longitudinal axis of the ship. Faltinsen [9] presented this method of evaluation of the viscous transverse force and moment, which will be characterised here as Version 1.

Version 1:
The cross flow principle assumes that:
- the flow separates due to cross flow past the ship,
- the longitudinal current components do not influence the transverse forces on a cross section and
- the transverse force on a cross section is mainly due to separated flow effects on the pressure distribution around the ship.

In this way the viscous transverse force may be presented as:

$$N_{vis} = \frac{1}{2} r \left[\int_{L_w} C_D(x) T_w(x) dx \right] U^2 \sin b \left| \sin b \right|$$

Equation 40

in which $C_D(x)$ is the cross flow drag coefficient for an infinite long cylinder with the cross sectional area of the ship at the longitudinal co-ordinate x and $T_w(x)$ is the sectional draught. If C_D is considered to be the average cross flow drag coefficient for the whole ship and T_w the constant draught, it may be written that for b up to 180^0:

$$N_{vis} = \frac{1}{2} r C_D T_w U^2 L_w \sin^2 b$$

Equation 41

In non-dimensional form, it looks like:

$$N'_{vis} = \frac{N_v}{\frac{1}{2} r U^2 L_w T_w} = C_D \sin^2 b$$

Equation 42

It follows from this expression that C_D may considered to be the amplitude of the viscous transverse force and may be presented as:

$$C_D = \frac{N'_{vis}}{\sin^2 b}$$

Equation 43

From Equation 40 it is clear that the viscous transverse moment may be presented as:

$$M_{vis} = \frac{1}{2} r \left[\int_{L_w} C_D(x) T_w(x) x dx \right] U^2 \sin b \left| \sin b \right|$$

Equation 44

Following the same reasoning as for the transverse viscous force, this equation for constant values of C_D and T_w may be transformed into:

$$M_{vis} = \frac{1}{4} r C_D T_w U^2 L_w^2 \sin^2 b$$

Equation 45

In non-dimensional form this viscous moment can be expressed as:

$$M'_{vis} = \frac{M_{vis}}{\frac{1}{2} r U^2 L_w^2 T_w} = \frac{1}{2} C_D \sin^2 b$$

Equation 46

According to Faltinsen [9], it should be kept in mind that the C_D values for the ship section considered are influenced by free surface effects, beam-draught ratio, bilge radius effects, bilge keel and effects of laminar or turbulent flow.

Equation 42 and Equation 46 show that the viscous transverse force and moment oscillate related to the drift angle with $\sin^2 b$ (up to $b = 180^0$). This means that for small drift angles (up to $b = 10^0$) the viscous force and moment vary with b^2. In this way this force and moment show a non-linear character with respect to drift angle b. It should be remembered that the potential transverse forces and moments show a linear relation to drift angle b in this region of small angles as shown in Section 2.2.2.

Version 2:

In the above mentioned Version 1, Faltinsen [9] assumed C_D as function of x, while Hoerner [20] also introduced $C_D(x)\sin b$ in case of cylinders with an angle of attack b for the cross flow. This implicates that viscous transverse forces and moments as derived in Equation 42 and Equation 46 oscillate with $\sin^3 b$. For small drift angles (up to $b = 10^0$) the viscous transverse force and moment vary with b^3, also being non-linear in character.

In case of negative drift angles, $\sin^3 b$ - essentially being $\sin^2 b|\sin b|$ - remains positive in sign.

2.4. Total transverse forces

Version 1:

From the preceding sections it should be clear that the total transverse force N_{tot} in general is found by summation of the potential and viscous force and so this force will be according to Equation 6 and Equation 41:

$$N_{tot} = N_{pot} + N_{vis} = \frac{1}{2}U^2 m'_{x_{mb}} \sin 2b + \frac{1}{2} r C_D T_w U^2 L_w \sin^2 b$$

Equation 47

The same reasoning holds for the total transverse moment, which may be expressed with Equation 9 and Equation 45 as:

$$M_{tot} = M_{pot} + M_{vis} = \frac{1}{2}U^2 m_D \sin 2b + \frac{1}{4} r C_D T_w U^2 L_w^2 \sin^2 b$$

Equation 48

There are to indicate two exceptions viz.:

1. The drift angle is rather small, so $b = 0^0 - 10^0$. In this case the viscous force may be neglected and only the potential force and moment should be accounted for as shown in Section 2.2.2. Equation 14 and Equation 15 should then be used for respectively transverse force and moment; see also Figure 1.
2. The drift angle b achieves a value between 80^0 and 90^0. In that case the potential transverse force and moment may be neglected and only the viscous force and moment should be taken into account. If for $b = 80^0 - 90^0$ the term $\sin^2 b$ is considered to be 1, this viscous force and moment as presented in Equation 41 and Equation 45 will then be respectively:

$$N_{vis} = \frac{1}{2} r C_D T_w U^2 L_w$$

Equation 49

$$M_{vis} = \frac{1}{4} rC_D T_w U^2 L_w^2$$

Equation 50

It should be kept in mind that, if e.g. the drift angles in manoeuvring are more than 10^0, viscous influence should be added to the expressions of Section 2.2.2.

Version 2:
It might be clear from the remarks about Version 2 in Section 2.3, that they also should be introduced into the expressions for the total transverse force and moment in Equation 47 and Equation 48 for the viscous component with $\sin^3 b$ instead of $\sin^2 b$.

3. Experiments

3.1. General

In the following sections reference will be made to experiments in the past with ship-like wing models [10,11,12,13] as well as to tests with a seven segments ship model also to measure the transverse forces [21] in deep and shallow water. At last will be presented the experimental results with the same segmented model to measure the transverse forces at 90^0 drift angle for several ship conditions in deep water only [22].

3.2. Tests with ship-like wing models

The present study is based on reports by the first author [11,12,13] on manoeuvring derivatives for a low aspect-ratio surface piercing wing model in deep and shallow water. It is also a follow up of a report describing the lift production of such a wing model [10].
In the physical model for predicting lift production and manoeuvring coefficients the ship is considered to be a wing profile with a very low aspect ratio. To determine the hydrodynamic manoeuvring coefficients forced horizontal motion tests with a Planar Motion Mechanism (PMM) were performed. The tests were carried out at three speeds in opposite directions in both deep and shallow water. The longitudinal and transverse forces on the wing model were measured as function of drift angle b to determine the hydrostatic manoeuvring coefficients and as function of forward speed to determine the hydrodynamic manoeuvring coefficients. These experiments were carried out for three draughts (aspect ratios) and four water depths including deep water. Additionally some tests were performed with faired tips of the bilge instead of the usual square tips to show the viscous influence for the latter condition.
From the measurements of the transverse forces and moments the hydrostatic and hydrodynamic manoeuvring coefficients were determined and presented as functions of respectively drift angle and forward speed. These results were compared with calculated values for small angles and displacements representing the linear behaviour in that region. Some of these results are presented in Figure 4 and Figure 5.

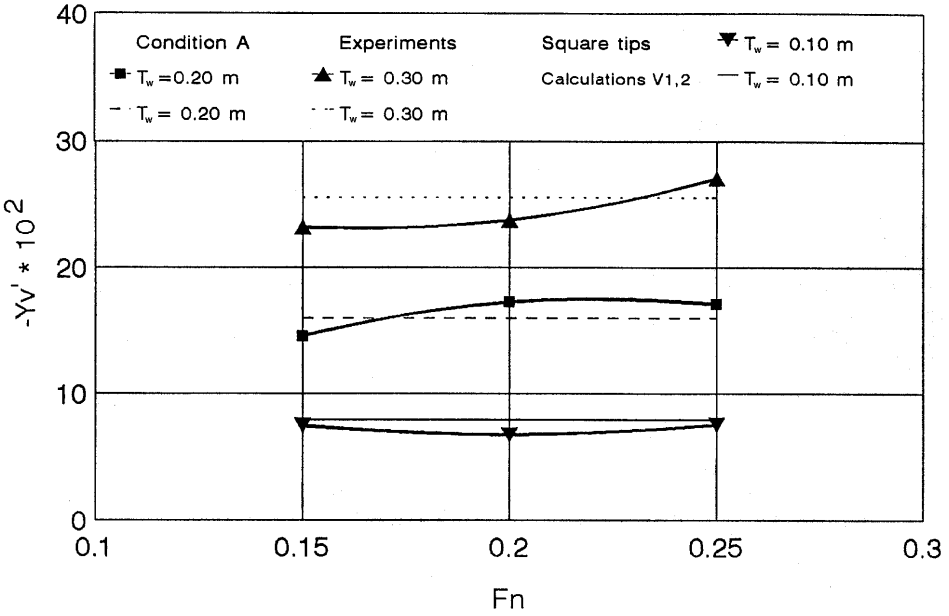

Figure 4 Measured and calculated –*Yv*' for sway, H/T_w = 1.2

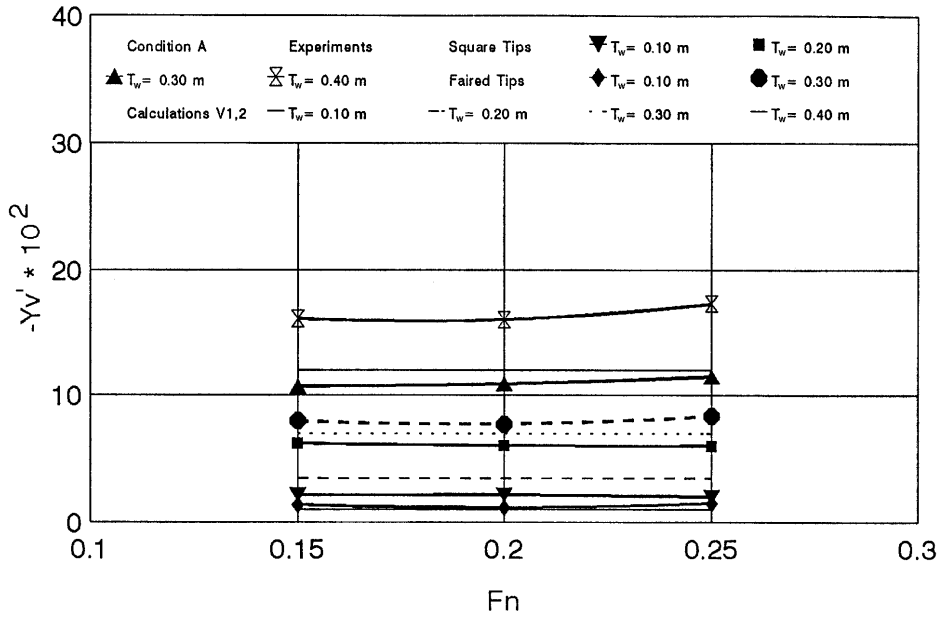

Figure 5 Measured and calculated –*Yv*' for sway, *H* = 2.50 m

Concerning the determination of the lift and drag force, it holds especially in case of a drift angle $b > 10^0$ (see Figure 2 and Section 2.2.3) for the measured values that:

$$N = L\cos b + D\sin b$$
$$T = D\cos b - L\sin b$$

Equation 51

from which the lift and drag follows as:

$$L = N\cos b - T\sin b$$
$$D = N\sin b + T\cos b$$

Equation 52

and in non-dimensional presentation:

$$C_L = \frac{L}{\frac{1}{2} r U^2 L_w T_w}$$

Equation 16

$$C_D = \frac{D}{\frac{1}{2} r U^2 L_w T_w}$$

Equation 53

As an example some of these measured results of C_L and C_D are shown in Figure 3 together with the calculated values. These calculated values are most times approaching the measured values for small drift angles and the condition with the faired tips of the bilge. If it is assumed that the calculated values are representing the potential lift, the difference with the experimental values should then show the viscous influence. In this way it is then possible to determine the C_D values with Equation 43. Table 2 shows for $b = 20^0$ and $Fn = 0.20$ the determination of these C_D values for the two Versions as denoted in Section 2.3.

H (m)	Square or Faired Tips	Exp. N'_{tot}	Calc. N'_{pot}	$N'_{vis} = N'_{tot} - N'_{pot}$	Version 1 C_D	Version 2 C_D
0.12	Square	1.002	0.522	0.480	4.103	11.996
0.16	Square	0.549	0.211	0.338	2.889	8.447
0.20	Square	0.431	0.147	0.284	2.428	7.099
0.60	Square	0.228	0.070	0.158	1.351	3.947
0.60	Faired	0.140	0.070	0.070	0.598	1.748
2.50	Square	0.199	0.070	0.129	1.103	3.225
2.50	Faired	0.142	0.070	0.072	0.616	1.801

Table 2 C_D values for the ship-like wing model, $b = 20^0$, $Fn = 0.20$

It is clear from this table that the C_D values increase with reduction of water depth and for the case of square tips of the bilge. The remarkable difference in C_D values between Version 1 and Version 2 is due to the difference in value of $\sin^2 b$ (Version 1) and $\sin^3 b$ (Version 2) at $b = 20^0$; see Figure 1 and Equation 43.

3.3. Tests with a segmented ship model

For a Todd 60 ($C_B = 0.70$) seven segments ship model, drift forces have been measured for drift angles up to 20^0 [21]. These experiments have been carried out for three different draughts and for the design draught also at $a = 3.4^0$ bow and stern trim. a is trim angle, bow down positive.

One condition with the design draught and $a = 0^0$ has also been investigated in shallow water, $H/T_w = 2.4$. The other conditions were related to deeper water, $H/T_w = 15$.

For each section (segment) the linear and non-linear part of the drift force have been determined as well as the cross flow drag coefficient C_D to find the longitudinal distribution of the coefficients related to speed, drift angle and sectional area coefficient. Similar relations have also been determined for the whole ship model.
It appeared that the forward sections contribute the most dominant part of the drift forces. Calculations, as proposed according to Equation 25, also taking into account the bottom influence and compared to the measured values derived from the linear part of the drift forces, show a rather good agreement for the forward part of the model until the section with the maximum beam, x_{mb}; see Figure 6.

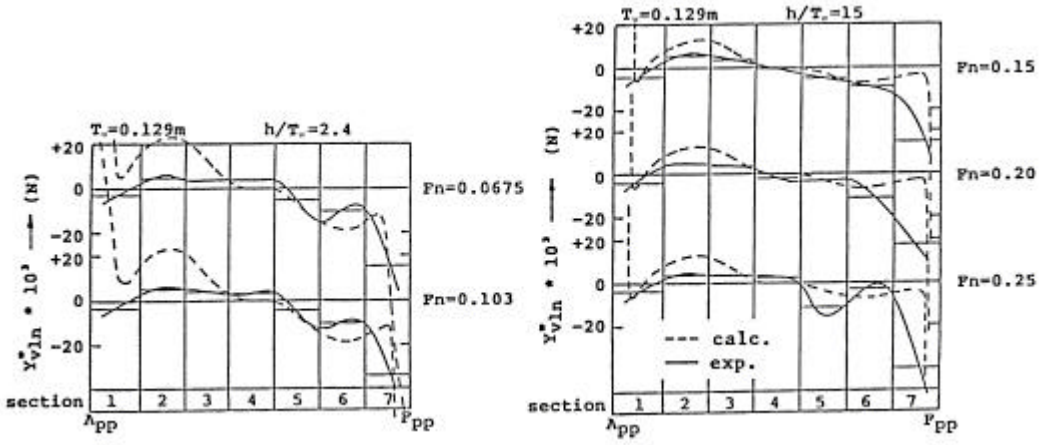

Figure 6 Longitudinal distribution of the non dimensional linear drift force

The sum of the sectional values deliver for the whole model:

- Y'_v for the total non-dimensional drift force,
- $Y'_{v\ln}$ as the linear component and
- Y'_{vnl} as the non-linear component of the total drift force.

Here is:

$$Y_v = \frac{Y}{v} = \frac{Y}{-U \sin b}$$

Equation 54

in which U is the forward speed and $v = -U \sin b$ is the transverse speed component.
The non-dimensional expression becomes:

$$Y'_v = \frac{Y_v}{\frac{1}{2} r L_w^2 U} = -\frac{Y}{\frac{1}{2} r L_w^2 U^2 \sin b}$$

Equation 55 (equal to Equation 26)

The total non-dimensional drift force will be:

$$Y'_v = Y'_{v\ln} + Y'_{vnl}$$

Equation 56

The cross flow drag coefficient according to Version 1 of Section 2.3 is:

$$C_D = \frac{Y_{nl}}{\frac{1}{2} r L_w T_w U^2 \sin b |\sin b|}$$

Equation 57

from which follows for $b < 180^0$ with Equation 55:

$$C_D = -Y'_{vnl} \cdot \frac{L_w}{T_w \sin b}$$

Equation 58

For Version 2, this expression becomes:

$$C_D = -Y'_{vnl} \cdot \frac{L_w}{T_w \sin^2 b}$$

Equation 59

The measured and derived values are shown in Table 3 and Figure 7 for the denoted conditions:

Fn = 0.20 U = 0.941 m/s					
β (deg)	Y'_v *10^3	$Y'_{v\ln}$ *10^3	Y'_{vnl} *10^3	C_D	
				Version 1	Version 2
20	-23.2	-14.9	-8.3	0.434	1.268
16	-20.6	-14.9	-5.7	0.367	1.335
12	-18.4	-14.8	-3.6	0.306	1.469
8	-17.8	-16.1	-1.7	0.213	1.525

Table 3 Cross flow drag coefficient C_D from measured forces for the whole model, T_w = 0.129 m, a = 0^0, H/T_w = 15

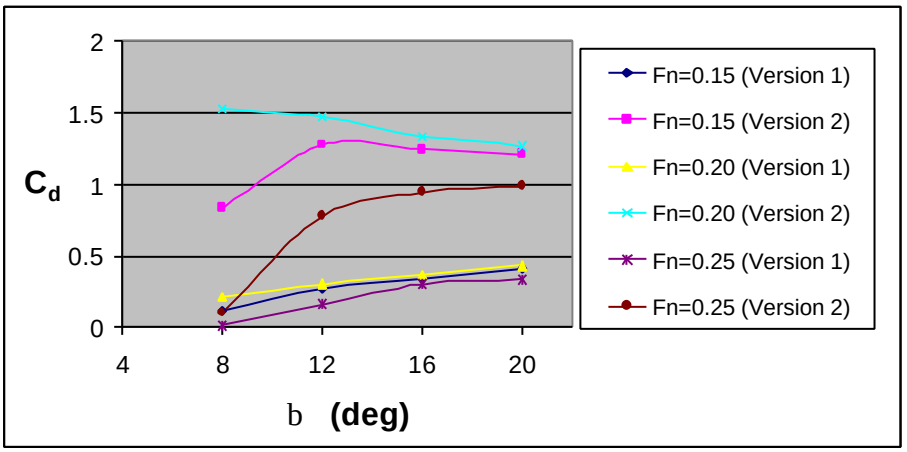

Figure 7 Cross flow drag coefficient C_D for the whole model as function of drift angle

3.4. Tests with a segmented ship model at 90 degree drift angle

This investigation is a rational follow up of previous research (see Section 3.3.) in which for a seven segments ship model drift forces have been measured for drift angles up to 20^0 at different forward speeds [21].
In this case a drift angle of 90^0 has been taken into consideration for the same ship model to measure the drift forces at values of transverse speed corresponding to the transverse speed component, occurring during the preceding above mentioned tests. These experiments as well as the present ones have been carried out for three different draughts and for the design draught at $a = +3.4^0$ bow and $a = -3.4^0$ stern trim.
These static drift experiments at 90^0 drift angle were carried out with the 2.3 m model of the Todd 60 Series. The main particulars are presented in Table 4.

Length between perpendiculars	L_{pp}	2.258 m
Length on the waterline	L_w	2.296 m
Beam	B_w	0.322 m
Draught	T_w	0.129 m
Block coefficient	C_B	0.70

Table 4 Main particulars of the seven segments Todd Sixty Model

The model has been tested without rudder and propeller. The same model has been used for the experiments as described in Section 3.3. The position of the model at 90^0 drift angle was such that the port side was in the towing direction. For the design condition all sections have a length l_s = 0.323 m, except section no. 1 which has a length l_s = 0.360 m. The test conditions are summarised in Table 5. The forward speed has been adjusted up to a maximum of 0.50 m/s in steps of 0.10 m/s. This maximum speed corresponds to the transverse speed at the maximum drift angle of 20 degrees and the maximum forward speed $Fn = 0.25$, as used in the preceding research. For each section the total drift force Y_{nl}^* has been measured assuming that the potential force $Y_{\ln}^*$ was zero at 90^0 drift angle.

Cond. No.	Draught T_w (m)	Length L_w (m)	Trim a (deg)	Water-Depth Draught Ratio H/T_w
1	0.129	2.296	0	15
2	0.129	2.233	+3.4 (Bow down)	15
3	0.129	2.314	-3.4 (Bow up)	15
4	0.159	2.320	0	12
5	0.099	2.216	0	20

Table 5 Test conditions

The cross flow drag coefficient for each section is, analogous to Equation 57, defined as:

$$C_D^* = \frac{Y_{nl}^*}{\frac{1}{2} r L_w T_w^* U^2}$$

Equation 60

Analogous to Equation 58, it is found for both Versions 1 and 2 ($\sin b = 1$):

$$C_D^* = -Y_{vnl}^{*'} \cdot \frac{L_w}{T_w^*}$$

Equation 61

and for the whole model:

$$C_D = -Y'_{vnl} \cdot \frac{L_w}{T_w}$$

Equation 62

Test results are for one denoted condition as an example shown in Table 6.

U (m/s)	C_D^* Section No.							C_D
	1	2	3	4	5	6	7	
.05	.30	.24	.19	.13	.22	.16	.27	1.51
.10	.24	.19	.18	.15	.19	.18	.23	1.36
.20	.22	.18	.16	.14	.16	.16	.20	1.22
.30	.22	.18	.15	.14	.15	.17	.21	1.22
.40	.22	.19	.15	.12	.15	.17	.22	1.22
.50	.22	.17	.14	.12	.14	.17	.22	1.18

Table 6 Cross flow drag coefficients at 90^0 drift angle

Condition No. 1, L_w = 2.296 m, T_w^* = 0.129 m, a = 0^0, H/T_w = 15

It should be remarked that the results for C_D at 90^0 drift angle in case of the transverse component for $Fn = 0.20$ at 20^0 drift angle ($U = v$ = 0.325 m/s) show a value of 1.22 for C_D. This agrees rather well with the results found for Version 2 in Table 3 for the mentioned condition, being there $C_D = 1.268$, while Version 1 in general show too low values. The C_D values for the ship-like wing model (see Table 2) show - for $Fn = 0.20$ and drift angle $b = 20^0$ in deep water with faired bilge tips - rather high values in case of Version 2, viz. C_D values of 1.92 and 1.75. Up to now, it is unknown how deviations from the real ship form influence the C_D values.

It should be noticed also that, according to the results in Table 6, the values for C_D increase with speed reduction.

The longitudinal distribution of C_D is presented in Figure 8 for U = 0.30 m/s and the denoted conditions with a horizontally drawn line representing the average value of each segment and is defined as:

$$C'_D = \frac{C_D^*}{l_s}$$

Equation 63

where l_s is the length of the segment under consideration.

A possible continuous curve for the coefficient C'_D is suggested in Figure 8 by taking into account the condition that for each segment the average value should be reproduced.

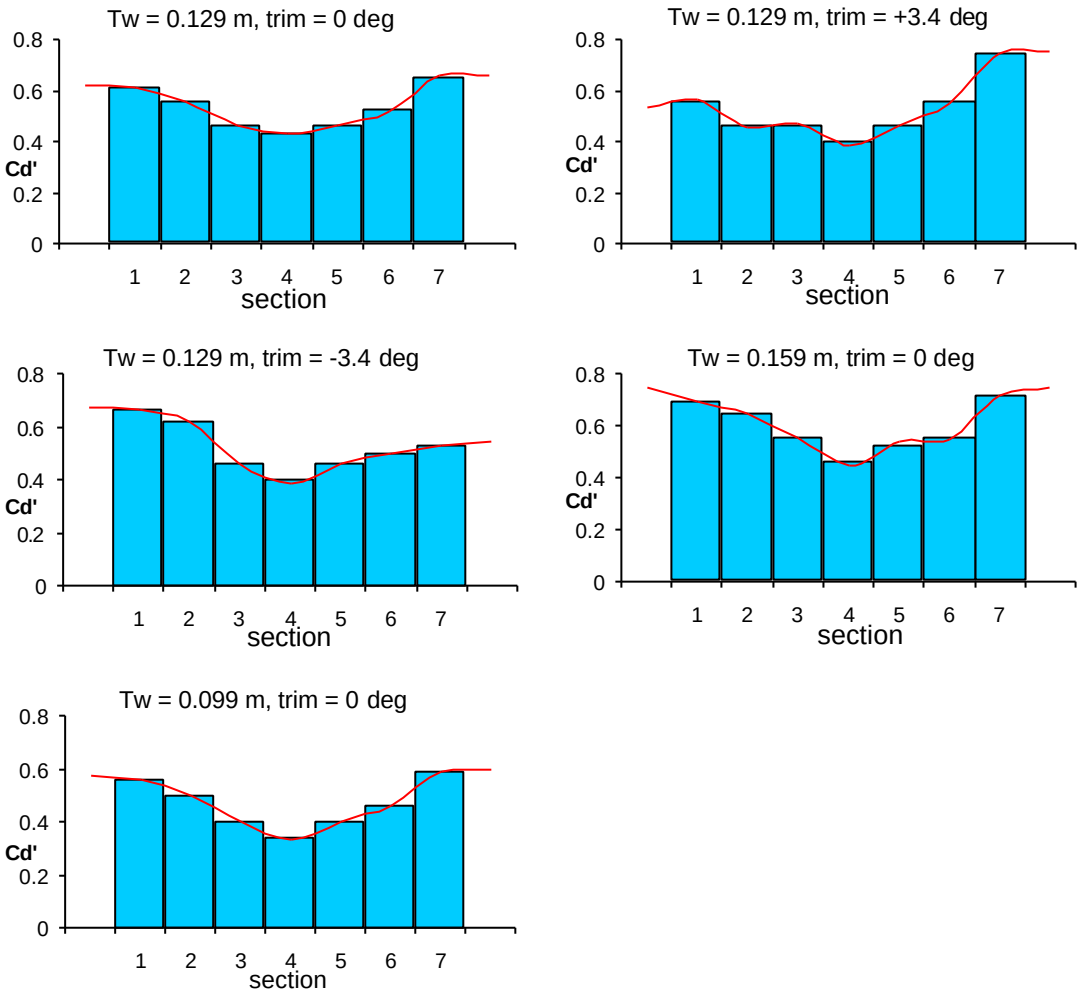

Figure 8 Longitudinal distribution of C_D at 90^0 drift angle for U = 0.30 m/s

4. Conclusions

The presented calculation method to determine lift production and manoeuvring derivatives and the method to calculate the viscous drag, deliver - compared to the described test results - the following conclusions:

1. Reduction of water depth causes a strong increase of transverse forces and moments as shown by experiments. Calculated values confirm this very well.

2. Using faired tips at the bilge instead of square tips decrease drag and transverse force considerably and approach rather close the calculated potential values.

3. The presented calculation method supplies a useful tool to determine the manoeuvring coefficients for deep and shallow water showing good agreement with measurements and results of semi-empirical methods for ships in deep water. For drift angles larger than 10^0 the influence of viscous transverse forces should be taken into account.

4. The drift angular dependence for the potential transverse forces appears to be according to $\sin 2b$. At small angles up to $b = 10^0$ this dependence may be considered to be linear with the drift angle b and may be applied for manoeuvring situations. The maximum value of the potential transverse force will be achieved at drift angle $b = 45^0$.

5. The viscous transverse force has a drift angular dependence according to $\sin^2 b$ (Version 1) or to $\sin^3 b$ (Version 2) which for small drift angles ($b < 10^0$) may be considered to be respectively b^2 or b^3, showing in this way a non-linear character in this region. The maximum value of the viscous transverse force will be achieved at a drift angle $b = 90^0$, where the potential transverse force will be zero in value. For $b = 80^0 - 90^0$ the potential transverse force and moment may be neglected. Determination of the cross flow drag coefficient C_D from tests at small drift angles shows the best results for Version 2 if compared to the test results for 90^0 drift angle.

6. Experiments with a segmented model at 90^0 drift angle show a rather equal distribution of the cross flow drag coefficient C_D over the ship length. This coefficient C_D is almost constant with speed except for the low speed region ($Fn = 0.02$) where the value of C_D increases.

5. Appendix

This Appendix gives an overview of the sway and yaw coefficients.

$Y_v = U\int_{x_{mb}}^{F}\frac{dm'}{dx}dx = -Um'_{x_{mb}}$	$Y'_v = \frac{Y_v}{\frac{1}{2}rL_w^2U} = \frac{-m'_{x_{mb}}}{\frac{1}{2}rL_w^2}$
$Y_{\dot v} = -\int_{A}^{F} m'dx$	$Y'_{\dot v} = \frac{Y_{\dot v}}{\frac{1}{2}rL_w^3} = \frac{1}{\frac{1}{2}rL_w^3}\int_{A}^{F} m'dx$
$N_v = \int_{x_{mb}}^{F}\frac{dm'}{dx}xdx$	$N'_v = \frac{N_v}{\frac{1}{2}rL_w^3U}$
$= U\left[-x_{mb}m'_{x_{mb}} - \int_{x_{mb}}^{F} m'dx\right]$	$= \frac{1}{\frac{1}{2}rL_w^3}\left[-x_{mb}m'_{x_{mb}} - \int_{x_{mb}}^{F} m'dx\right]$
$N_{\dot v} = -\int_{A}^{F} m'xdx = Y_{\dot r}$	$N'_{\dot v} = \frac{N_{\dot v}}{\frac{1}{2}rL_w^4} = -\frac{1}{\frac{1}{2}rL_w^4}\int_{A}^{F} m'xdx = Y'_{\dot r}$

Table 7 Overview of sway coefficients

$Y_r = U\left[\int_{x_{mb}}^{F} \frac{dm'}{dx} x dx + \int_{A}^{F} m' x dx\right]$ $= U\left[-x_{mb} m'_{x_{mb}} - \int_{x_{mb}}^{F} m' dx + \int_{A}^{F} m' dx\right]$	$Y'_r = \frac{Y_r}{\frac{1}{2} r L_w^3 U}$ $= \frac{1}{\frac{1}{2} r L_w^3}\left[-x_{mb} m'_{x_{mb}} - \int_{x_{mb}}^{F} m' dx + \int_{A}^{F} m' dx\right]$ $= N'_v - Y'_{\dot{v}}$
$Y_{\dot{r}} = -\int_{A}^{F} m' x dx = N_{\dot{v}}$	$Y'_{\dot{r}} = \frac{Y_{\dot{r}}}{\frac{1}{2} r L_w^4} = \frac{1}{\frac{1}{2} r L_w^4} \int_{A}^{F} m' x dx = N'_{\dot{v}}$
$N_r = U\left[\int_{x_{mb}}^{F} \frac{dm'}{dx} x^2 dx + \int_{A}^{F} m' x dx\right]$ $= U\left[-x_{mb}^2 m'_{x_{mb}} - 2\int_{x_{mb}}^{F} m' x dx + \int_{A}^{F} m' x dx\right]$	$N'_r = \frac{N_r}{\frac{1}{2} r L_w^4 U}$ $= \frac{1}{\frac{1}{2} r L_w^4} * \left[-x_{mb}^2 m'_{mb} - 2\int_{x_{mb}}^{F} m' x dx + \int_{A}^{F} m' dx\right]$ $= \frac{1}{\frac{1}{2} r L_w^4}\left[-x_{mb}^2 m'_{x_{mb}} - 2\int_{x_{mb}}^{F} m' x dx\right] - Y'_{\dot{r}}$
$N_{\dot{r}} = -\int_{A}^{F} m' x^2 dx$	$N'_{\dot{r}} = \frac{N_{\dot{r}}}{\frac{1}{2} r L_w^5} = -\frac{1}{\frac{1}{2} r L_w^5} \int_{A}^{F} m' x^2 dx$

Table 8 Overview of yaw coefficients

6. References

1. Jones, R.T. (1945), *Properties of Low Aspect-ratio Pointed Wings at Speeds Below and Above the Speed of Sound*, NACA-Report 835.
2. Payne, P.R. (1992), *A Unification in the Added Mass Theory of Planing*, Ocean Engineering, Volume 19, No. 1, pp. 39-45, United Kingdom.
3. Newman, J.N. (1977), *Marine Hydrodynamics*, Book, MIT Press, Cambridge, Massachusetts, USA.
4. Keil, H. (1974), *Die Hydrodynamische Kräfte bei der Periodische Bewegung zwei-dimensionaler Körper an der Oberfläche flacher Gewasser*, Institut für Schiffbau der Universität Hamburg, Bericht No. 305.
5. Journée, J.M.J. (2001), *Theoretical Manual of SEAWAY, Release 4.19*, Report 1216a, February 2001, Delft University of Technology, Ship Hydromechanics Laboratory, Delft, the Netherlands.

Internet: *TheoreticalManualSEAWAY.pdf* in Section "Ship Motions Program SEAWAY" at website www.shipmotions.nl.
6. Dmitrieva, Dr. I., *Numerical Investigations of Motions and Drift Forces on Different Bodies Using DELFRAC Program*, Report 1016, Ship Hydromechanics Laboratory, Delft University of Technology, the Netherlands.
7. Koning Gans, H.J. de (1994), *Numerical Time Dependent Sheet Cavitation Simulation using a Higher Order Panel Method*, Ph.D. Thesis, Delft University Press, ISBN 90-6275-965-3, the Netherlands.
8. Katz, J. and Plotkin, A. (1991), *Low Speed Aerodynamics, from Wing Theory to Panel Methods*, McGraw-Hill, International Editions.
9. Faltinsen, O.M. (1990), *Sea Loads on Ships and Offshore Structures*, Book, Cambridge University Press, ISBN 0 521 37285 2.
10. Beukelman, W. (1993), *Lift and Drag for a Low Aspect-ratio Surface Piercing Wing Model in Deep and Shallow Water*, ISBN 90-370-0095-9, Ship Hydromechanics Laboratory, Delft University of Technology, the Netherlands.
11. Beukelman, W. (1995), *Manoeuvring Derivatives for a Low Aspect-ratio Surface Piercing Wing Model in Deep and Shallow Water*, (MEMT, ISNN0925-6555 No.35), ISBN 90-370-0127-0, Ship Hydromechanics Laboratory, Delft University of Technology, The Netherlands.
12. Beukelman, W. (1998), *Manoeuvring Coefficients for a Wing Model in Deep and Shallow Water*, International Shipbuilding Progress, Volume 45, No.441, Delft University Press, the Netherlands.
13. Beukelman, W. (1996), *Fluid Momentum in Ship Hydrodynamics*, CRF-96, Transactions of the Third International Conference in Commemoration of the 300th Anniversary of Creating Russian Fleet by Peter the Great, St. Petersburg, State Marine Technical University.
14. Leeuwen, G. van and Journée, J.M.J., (1972), *Prediction of Ship Manoeuvrability*, Report 158-S, Netherlands Ship Research Centre TNO, Delft, the Netherlands.
    Internet: *0288-TNO-158S.doc* in Section "Papers and Reports" at website www.shipmotions.nl.
15. Norrbin, N.H. (1971), *Theory and Observations on the Use of a Mathematical Model for Ship Manoeuvring in Deep and Confined Waters*, Swedish State Shipbuilding Experimental Towing Tank, Publication 68, 1971.
16. Gerritsma, J., Beukelman, W. and Glansdorp, C.C., (1974), *The Effect of Beam on the Hydrodynamic Characteristics of Ship Hulls*, 10th Office of Naval Research Symposium, Boston, USA or Report No. 403-P, Ship Hydromechanics Laboratory, Delft University of Technology, the Netherlands.
17. Inoue, S., Hirano, M. and Kijima, K. (1981), *Hydrodynamic Derivatives on Ship Manoeuvring*, International Shipbuilding Progress, Volume 28, No.321, May 1981,The Netherlands.
18. Clarke, D., Gedling, P. and Hine, G. (1982), *The Application of Manoeuvring Criteria in Hull Design Using Linear Theory*, Transactions RINA, 1982.
19. Book: *Principles of Naval Architecture, Volume III: Motions in Waves and Controllability*, The Society of Naval Architects and Marine Engineers, New York, USA.
20. Hoerner, S.F. (1965) *Book: Fluid-Dynamic Drag*, Hoerner, Fluid Dynamics, P.O. Box 342, Brick Town, N.J.08723, USA.
21. Beukelman, W. (1989), *Cross Flow Drag on a Segmented Model*, Fourth International Symposium on Practical Design of Ships and Mobile Units (PRADS89), Varna, Bulgaria.

22. Beukelman, W. (1989), *Distribution of Drift Forces at 90 Degree Drift Angle*, Papers on Shiphydromechanics, Volume V, Ship Hydromechanics Laboratory, Delft University of Technology, the Netherlands.